Lab on a Chip

This is an *Accepted Manuscript*, which has been through the Royal Society of Chemistry peer review process and has been accepted for publication.

Accepted Manuscripts are published online shortly after acceptance, before technical editing, formatting and proof reading. Using this free service, authors can make their results available to the community, in citable form, before we publish the edited article. We will replace this *Accepted Manuscript* with the edited and formatted *Advance Article* as soon as it is available.

You can find more information about *Accepted Manuscripts* in the **Information for Authors**.

Lab on a Chip

ARTICLE

Modular microfluidics for point-of-care protein purifications

L. J. Millet,*[1,2] J. D. Lucheon,[1] R. F. Standaert,[1,2] S. T. Retterer,[1,2] and M. J. Doktycz[1,2]

Biochemical separations are the heart of diagnostic assays and purification methods for biologics. On-chip miniaturization and modularization of separation procedures will enable the development of customized, portable devices for personalized health-care diagnostics and point-of-use production of treatments. In this report, we describe the design and fabrication of miniature ion exchange, size exclusion and affinity chromatography modules for on-chip clean-up of recombinantly-produced proteins. Our results demonstrate that these common separations techniques can be implemented in microfluidic modules with performance comparable to conventional approaches. We introduce embedded 3-D microfluidic interconnects for integrating micro-scale separation modules that can be arranged and reconfigured to suit a variety of fluidic operations or biochemical processes. We demonstrate the utility of the modular approach with a platform for the enrichment of enhanced green fluorescent protein (eGFP) from *Escherichia coli* lysate through integrated affinity and size-exclusion chromatography modules.

1. Introduction

Production and characterization of recombinant proteins are integral to a variety of fundamental and applied studies. With advances in DNA sequencing technology has come an explosion of genomic DNA sequence data, from which a seemingly unlimited number of natural proteins and variants could be produced. Advances in DNA synthesis technology and molecular biology have simplified construction of appropriate DNA sequences for expression of these proteins.[1,2] However, production and characterization of proteins remains a bottleneck. To exploit the wealth of possibilities, there is a pressing need to process small-volume samples efficiently[3,4] and to prepare and analyze small quantities of recombinant proteins. Operating at reduced scale is necessary for space- and cost-effective screening of protein activity and for evaluating the expression, purification and assay conditions needed for larger scale manufacture.[5–9]

The ability to prepare small quantities of pure proteins on demand will also prove valuable for emerging applications focused on the portable manufacture of biologic medicines. Delivering sensitive therapeutic proteins to resource-limited

environments and maintaining their stability may be impossible, in which case making such proteins at the point of need would be required, and where on-demand biochemical synthesis could complement the utility of point-of-care diagnostic platforms.[10,11]

Recombinant proteins are produced through a variety of means. Most commonly, proteins are expressed in a prokaryotic host, such as *E. coli*. Certain proteins require posttranslational modification or do not fold properly in prokaryotic hosts, and thus must be produced in eukaryotic cell lines.[12] Alternatively, cell-free synthesis techniques can be employed.[8,13,14] Despite the wide variety of production methods, purification schemes comprise a relatively small set of basic tools. Commonly, chromatographic separations that employ general or selective binding, such as ion exchange or affinity techniques, are combined with methods for size selection to separate the product from larger or smaller proteins, as well as salts, buffers and other small molecules. The order, exact implementation, and appropriate combination of these broadly applicable chromatographic tools can be varied to afford the protein of interest with the desired purity.[1]

Technologies for miniaturizing and automating the process of protein purification remain immature. In this regard, microfluidic-based approaches are well suited to meet the demands associated with multi-step purification in small-scale protein production.[15–17] The inherent scale and simple production of systems based on this technology contribute to

[1] Biological and Nanoscale Systems Group, Biosciences Division, Oak Ridge National Laboratory, PO Box 2008 MS 6445, Oak Ridge, TN 37831-6445
[2] The Center for Nanophase Materials Sciences, Oak Ridge National Laboratory, PO Box 2008 MS 6445, Oak Ridge, TN 37831-6445
*E-mail: milletlj@ornl.gov

the feasibility of creating portable, disposable systems and for integrating various chromatographic processes onto a single device. The scale of microfluidic devices also enables the exploration of novel approaches for separating and concentrating proteins.[18–22] As purification devices are miniaturized, they can be mated with scale-compatible devices for characterization and functional screening[23–25] to afford further advantages, such as efficiency, reliable sample tracking, and reduced potential for contamination or degradation.

In this report, we describe the design, fabrication and functional integration of protein chromatography modules to effect the isolation of recombinantly expressed protein (Figure 1). Conventional chromatography matrices were utilized for on-chip protein separations.[26] Microfluidic ion exchange chromatography is used for concentrating and fractionating samples,[18,27] microfluidic size-exclusion chromatography is used for exchanging buffers, desalting proteins, and for cell/particle size separations.[28–30] Microfluidic affinity chromatography is used to separate cells and molecules containing specific ligands,[31–33] in metal affinity chromatography ligands on the protein selectively bind to metal ion-functionalized separation media for increased purification.[26] The operational parameters for microfluidic process scaling were evaluated and are discussed herein. Integration of microfluidic modules through 3-D fluidic bridges is described and applied to *E. coli* lysates for on-chip purification of eGFP.
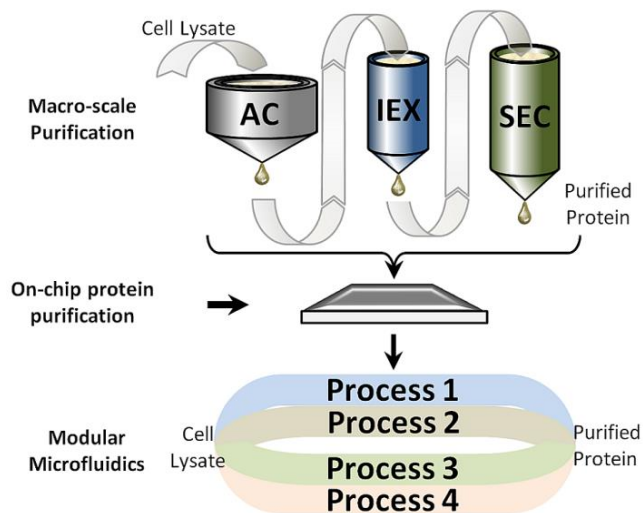
Figure 1. Biochemical separations of recombinant proteins are scalable. Affinity chromatography (AC), ion exchange chromatography (IEX), and size exclusion chromatography (SEC) are common approaches used in biochemical cleanup processes. Macroscale analytical chemical processes are used for purifying protein-based therapeutics (top). Modularization of protein purification strategies using microfluidics for scalable biochemical separations of recombinant proteins is possible. Microfluidics enable scaling down biochemical separations for on-chip protein purifications (middle). The modularization of protein purification steps into a single integrated platform allows for reconfiguring the purification steps on-chip to enable multiple different purification processes (bottom).

2. Experimental

2.1. Photolithography

Soda lime chrome masks for lithographic patterning of microfluidics devices were fabricated in house using five-inch soda lime plates pre-coated with AZTFP-650 photoresist (Nanofilm). Glass plates were exposed on a Heidelberg Instruments DWL 66 mask writer using either a 4 mm or a 20 mm write head. Exposed masks were developed for 1 minute in CD-26 developer, rinsed with DI-water and dried with nitrogen. Exposed chrome was removed by immersing the plates CR14S for 2 min, then rinsing them with deionized water and drying them with nitrogen.

Silicon wafers with a 1.0 μm thermal silicon dioxide layer were used as starting material for masters on which microfluidic modules were cast. Wafers were spin-coated with MicroPrime P20 adhesion promoter (Shin-Etsu Microsci) followed by a 2–3 μm thick layer of SPR220 photo resist, soft baked (115 °C, 90 s), exposed (365-nm light), baked (115 °C, 90 s), and then developed (CD-26). A reactive ion etch (RIE) was used to remove the exposed oxide from the silicon. The remaining photoresist was removed by sonication in acetone followed by solvent and water rinses, and a 30 min resist-strip process (TepLa Ion Wave 10 plasma processing system) to reveal the oxide etch mask. The exposed silicon surface was etched with a modified Bosch process to produce a microfluidic channel structure with a depth of about 130 μm. Wafers were then plasma treated (air plasma, 2 min.) immediately prior to silane coating with trichloro(1H,1H,2H,2H-perfluoro-*n*-octyl)silane. Silanization was performed by placing the wafer in a closed glass Petri dish (120 mm) containing 20 μL of silane in a detached microvial cap, and heating the Petri dish on a hot plate (85 °C, 1–2 hr) inside a fume hood.

2.2. Replica molding of microfluidic modules.

To form fluidic access ports, Silastic tubing (Helix Medical) was affixed to sites of fluidic access on the silanized master using Duco cement (dry 10-15 min, room temperature).[34] To form fluidic bridges, acrylonitrile butadiene styrene (ABS) filaments were used in place of Silastic tubing. PDMS pre-polymer and curing agents were mixed, poured only around the base of the tubing and ABS filaments, and then cured (70 °C, 15 min). With tubing and filaments secured by cured PDMS, the Petri dish was filled with liquid PDMS, degassed under vacuum and cured (70 °C, 30 min) to complete the molding process.

PDMS replicas containing embedded tubing and ABS filaments were cut and removed from the wafer. Duco cement adheres well to ABS, but not PDMS or the silanized wafer. Thus, the PDMS was lifted from the wafer, and the cement plugs were removed from the underside of the PDMS and tubing to open the fluidic ports. The ends of the ABS filaments containing Duco cement were cut off to allow the filament to be retracted through the polymerized PDMS. The PDMS microfluidic channel (containing the ABS filament) was

lubricated with isopropyl alcohol, fine tip forceps were used to withdraw ABS filaments out of the cured PDMS to leave the cast-in-place fluidic channels that act as a fluidic bridge over other microfluidic structures. PDMS replicates were cleaned (3M Scotch Magic tape), plasma treated (air plasma, 2 min), attached to microscope slides (cleaned by wiping with isopropyl alcohol followed by a 2-min air plasma treatment), and baked (70 °C, 1 hr).

2.3. Packing modules with chromatography media.

Prior to priming the microfluidic channels with fluid, the PDMS microfluidic module was placed under vacuum for > 5 min to degas the PDMS. Microfluidic priming was achieved by removing the PDMS microfluidics from the vacuum chamber, adding degassed ethanol in distilled water (30%, v/v) to the inlet port and leaving undisturbed for 20 min for PDMS to eliminate any residual bubbles from channels. Ethanol was exchanged with degassed distilled water to remove the ethanol.

To pack the water-filled separation chambers in the microfluidic modules, pre-hydrated filtered beads (in water) were added to a pipette tip (1-mL) inserted into the silastic tubing of the chromatography medium input port of the device. With the module held at nearly a vertical (75-80 degree angle) position (inlet above outlet), gravity pulled the water and beads into the separation chamber, the beads were retained by microporous barriers built into the end of the bed. Peristaltic manipulation of the highly elastic, silastic tubing can be used to assist in bead loading of the separation chamber. Peristaltic manipulations are particularly helpful in finishing the bead loading process when the fluidic resistance increases and as the chamber is nearly filled to capacity. A wet blunt end object was sometimes used to tap on the microfluidic device to dislodge beads that attach in the channel before packing is complete. After filling the separation chamber to capacity, the tubing to the chromatography medium input port was clamped shut with hemostats, and the bed was further packed by rinsing with water (1 mL) introduced through the sample inlet port.

2.4. Size-exclusion chromatography (SEC) microfluidic module.

Sephadex G25 beads (fine grade, 20-80 μm dia., dry) were swollen with distilled water (31-125 μm dia., hydrated) and filtered through a cell strainer (70 μm mesh) to resize the beads for the bed thickness (110-120 μm).

A range of pressure head heights was achieved by using pipette tips of different length (4.7 cm or 10 cm), or by attaching a serological pipette (10 mL) to the tip for greater head heights (20 cm and 30 cm). After initial flow rates were defined, the sample inlet port was fitted with flexible tubing connected to syringe pumps. Samples for desalting were loaded into the inlet tubing, while fractions of eluate were collected and retained in a 384-well plate for analyses.

2.5. Ion exchange (IEX) microfluidic module.

The device was primed and loaded with chromatography medium using the same process described above; the total bed volume was 11-12 μL. To concentrate protein, the stationary phase IEX medium was diethylaminoethanol (DEAE)-sepharose Fast Flow (GE Healthcare), the mobile phase running buffer was 0.05 M Tris–HCl (pH 7.4), and the elution buffer was 2.0 M NaCl. Flow was effected with a syringe pump operating at 4 μL/min. Module binding capacity was determined with bovine serum albumin (BSA); eluate fractions (5 or 10 μL each) were combined to determine the total protein content.

2.6. Protein quantification.

The protein concentration was determined using the Bradford assay (BioRad #500-0205) using bovine serum albumin (BSA) (4 μg/ml to 20 μg/ml) as standard and/or by measuring absorbance at 280 nm (A_{280}, eGFP extinction coefficient = 19770 M^{-1} cm^{-1}). Controls were performed to confirm agreement between these protein assays.

2.7. Column efficiency analysis.

The total binding capacity of the IEX module was determined by obtaining a breakthrough curve, followed by elution of the protein (2.0 M NaCl) and quantitation (A_{280}, Bradford).

Column efficiency for SEC analysis was performed using a pulse test of eGFP (M_r 27,000), Allura Red AC, (Red 40, M_r 496) or LiBr (M_r 87) solutions in distilled water. The nominal size exclusion limit for Sephadex G25 is M_r = 5,000. From the chromatographic peak of Red 40, we measured the performance values of the height equivalent to one theoretical plate (HETP), the reduced plate height (h)

$$h = \frac{HETP}{d_P},$$

where d_P is the average particle diameter, and the asymmetry factor (A_S).[35]

The separation factor, alpha (α), derives from the relative measure of retention times for components eluting from a given column and is calculated to be greater than unity, that is, the retention time t_R of the later eluting component is divided by that of the earlier eluting component. Therefore, separation effectiveness is proportional to the value of α. In the size-exclusion system used in this purification module, the separation factor[35] is equivalent to:

$$\alpha = \frac{t_R Salt}{t_R Protein}.$$

Resolution provides another measure of the overall effectiveness of a separation between components and incorporates the peak width at the base of a chromatogram. Generally, a resolution value greater than one is considered to be an adequate separation. Here, resolution is equivalent to:

$$R = \frac{2(t_R Salt - t_R Protein)}{w_P Protein + w_P Protein},$$

where w_P is peak width at base.[35]

2.8. eGFP purification.

Recombinant eGFP was used for characterizing the SEC desalting and IEX concentration columns. Recombinant eGFP with an N-terminal hexa-histidine tag (His-tag) was expressed

in *E. coli* [TOP10 cells (Life Technologies, Inc.) transformed with pET3a vector + *E. coli* promoter upstream eGFP coding sequence containing an N-terminal His-tag] and purified using immobilized metal affinity chromatography (IMAC) using Co^{2+}-nitrilotriacetic acid (Co-NTA) resin as described previously.[36] eGFP was concentrated and rinsed (0.05 M tris, pH 7.4) of elution buffers using Amicon centrifugal ultrafiltration devices (0.5 mL, 3k MWCO, Millipore), and stored (-80 °C) until used. Protein purity was verified through SDS-PAGE on a 10% gel (Miniprotean TGX, BioRad) with tris-glycine running buffer. Protein bands were detected with Coomassie Brilliant Blue stain.

3. Results and discussion

Two main challenges had to be overcome in order to make modular microfluidic chromatography devices for scaled-down biochemical separations. First a modular separations chamber that could be easily packed to retain particulate chromatography media had to be developed. Second, a system for creating fluidic interconnects between modules to enable multi-column separations had to be created. We addressed the first challenge with a column design featuring a single-use packing port and micropatterned column ends containing microporous barriers to retain resin particulates (Figure 2). The second challenge was addressed by incorporating fluidic bridges into the PDMS casting. The result is an integrated platform for on-chip, multi-step separation of volume-limited samples, which we validated with commercial chromatography media for anion IEX, SEC, and IMAC separations.

3.1. Column design and packing.

Conventional columns typically consist of a glass, plastic or metal tube with porous supports for media at the inlet and/or outlet, and various plumbing arrangements to allow introduction of the sample and collection of fractions with minimal mixing, peak distortion, dilution and sample loss. Microfluidic chambers are pseudo two–dimensional, with heights on the order of 130 μm and lateral dimensions constrained to a maximum of 7.5–10 cm by the scale of conventional wafers and lithographic tools. This scale supports bed volumes on the order of tens to hundreds of microliters, and the capacity to purify proteins on scales up to the order of 1 mg. While we employed different bed configurations and geometries for different chromatographic modalities, the fundamental design was the same.

The ends of the chromatographic column bed were an important aspect of the design. To retain media, we fabricated microporous barriers into the flow path at both ends of the column (Figure 2A). These barriers consist of a line of rectangular (35 μm x 60 μm) obstacles in the flow path (7 mm width, 1.2 cm length) separated by gaps (45 μm) to allow fluid flow. Module architecture consists of a single inlet with divergent channels to distribute the fluid before entering the chromatographic bed; following the media bed, converging channels coalesce to form a single channel outlet.

Uniform flow in and out of the sample bed was achieved with a branched fluidic channel in which the inlet channel was split successively into pairs of narrower channels, such that multiple, uniformly distributed bifurcating channels load and collect sample immediately adjacent to the microporous barriers (Figure 3). Cross sectional channel area was kept constant to maintain volume, and geometry was defined to minimize corners where bubbles could be trapped. Because the sample flow path is designed to retain media, a separate port at the head of the column was incorporated into the design to introduce chromatography media into the bed (Figure 3).

To maintain a uniform bed depth and prevent collapse of the channel, a grid of square support posts (180 μm diameter, 1 mm pitch) was placed in the channel for larger bed geometries. Low-dead volume external connections to the fluidic channel were made by molding Silastic tubing into the device. Because
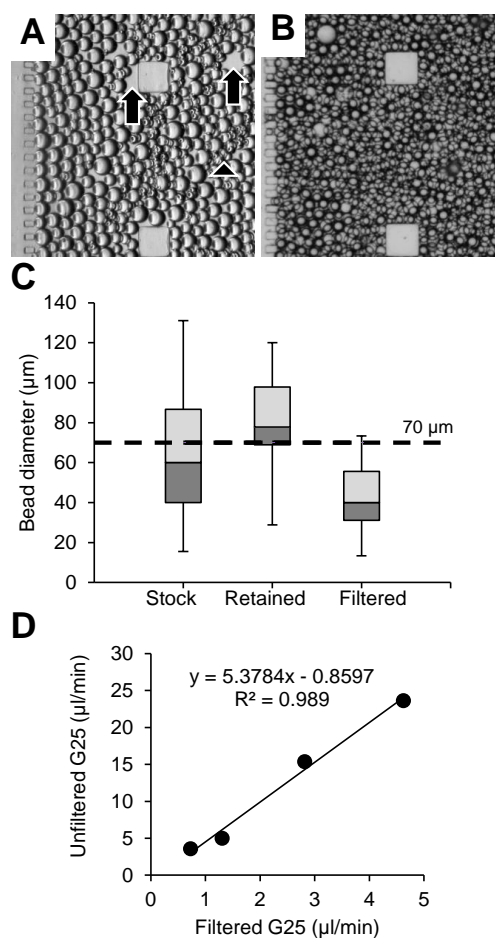
Figure 2. Size-matching chromatography beads to microfluidic structure for optimized module function. Bead diameter, uniform distribution, voids and bubbles influence flow uniformity, velocity and separation quality. A) Sedimentation layers (arrow heads) and voids (arrows) are observed when bead sizes approach or exceed the channel height. B-C) Media resizing (≤ 70 μm) near to half channel height improves bead packing. Box whisker plot shows the distribution (max., min., median and quartiles) of 70-μm filtered bead populations for ~130 μm tall channels. D) Flow rates are determined by bead size and packing quality; unfiltered beads packed in a microfluidic module produce about a five-fold higher increase (mean 4.8, s.d. 0.7) in flow rates as measured across four different pressure head heights (7.5, 10, 20, 30 cm).

Silastic tubing cross-links to the PDMS, the result is effectively a monolithic structure that forms durable robust connections devoid of leaks and forgiving of manual manipulation. The tubing is pliable and retains elastic properties, allowing for interchangeable connections to gravity-fed or pressure-fed systems (e.g. syringe pumps).

Bed packing strongly affects the quality of chromatographic processes, and the effects in the context of microfluidic devices have been analyzed thuroughly.[17] As in macroscale systems, bead packing at the surfaces of the bed sidewall (sphere to wall) produces larger fluid spaces than in the internal portion of the column, where tight packing occurs (sphere to sphere). The result is band broadening caused by non-uniform flow rates throughout the channel containing the chromatography bed.

Wall effects are a particularly serious concern in microfluidic devices due to the small channel height and overall large surface area-to-volume ratio of the chromatographic bed. To maximize chromatographic performance with SEC media, we sieved commercial chromatographic media using a 70-μm mesh to narrow the size distribution and use beads less than half channel height of ~130 μm to yield a chromatography bed ~2-4 bead layers thick. We employ this bead size to channel height criteria for improved separation; our in-house supply of size-exclusion media was resized through filtration for improved packing and performance (Figure 2). Specifically, Sephadex G-25 fine has a hydrated particle size distribution of 18–132 μm, which was reduced by sieving to 18–70 μm. In comparison to unsieved media, the sieved media gave tighter packing, had fewer voids, and afforded a 5-fold reduction in flow rate (Figure 2). For selective-adsorption media (ion-exchange and IMAC), adequate performance could be obtained without sieving.

Introducing beads into the microfluidic channel requires care due to the confined space and increased sidewall-area-to-bed-volume ratio. We were unable to pack the beds in one bulk loading; rather, dilute bead suspensions had to be added in successive fractions to avoid clogging the input tubing. Use of sieved beads reduced both clogging and particle size segregation by sedimentation during packing, such that more uniform packing is obtained. After packing, the media port was sealed by clamping the Silastic tubing. A tight packing is completed by perfusing the module with aqueous buffer or by standing the channels vertically for overnight settling. It is common for beads to settle after filling, thus reducing the 7 cm length to an effective 6.5 cm bead bed, as noted herein. Initially the tube sealing is reversible, after a few days of being clamped, the tubing seals irreversibly, disallowing repacking or bead addition after a few days of settling and use.

3.2. Ion exchange chromatography (IEX) modules.

Ion-exchange media have high adsorption capacities and chemical selectivity, making them useful for both gross and fine separations, as well as for concentrating charged analytes such as proteins from solution. Ion-exchange chromatography is accordingly a staple of protein purification. To achieve on-chip capture of proteins from small-volume samples, such as
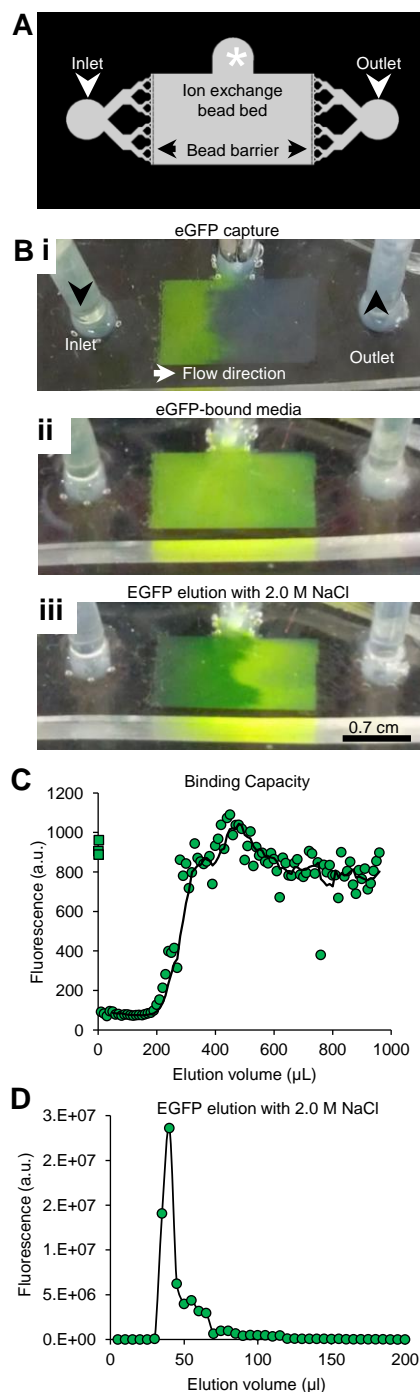
Figure 3. Microfluidic IEX module. A) Modular design for microfluidic IEX chromatography (1.2 cm (*l*) x 0.7 cm (*w*) x 0.011 cm (*d*), 11 μL bed volume). Design features consist of inlet and outlet ports (arrow heads), a media packing port (*), and microporous barriers (black arrows) to retain the media bed within the separation chamber. B) Capture of eGFP from a microfluidic module packed with DEAE sepharose. B.i.) Uniform capture of eGFP at the head of the bed is evident from the green color. B.ii.) The column is shown saturated with eGFP. B.iii.) The elution of eGFP with 2M NaCl. C) Breakthrough curve for bovine serum albumin (BSA) spiked with fluorescent tracer (eGFP). Green circles show eGFP fluorescence intensity in the eluted fractions (5 μL each), green squares show the measured fluorescence of the loading solution. Binding capacity (eGFP-spiked BSA) = 2.8 mg protein. D) Characteristic elution profile of eGFP off IEX module. Quantitative analysis showed the average elution of eGFP was 650 ± 162 μg (n=4) in ~35 μL of 2M NaCl.

50-µL *in-vitro* transcription/translation reactions, we fabricated microfluidic modules for ion-exchange chromatography on a scale for capturing ~1 mg protein. Because of the high binding capacity of IEX media for proteins up to 100 kDa (e.g., >100 mg of protein per mL of bed volume for Sepharose-type media), we fabricated a compact bed with dimensions of 0.7 × 1.2 × 0.013 cm (bed volume 11 µL) (Figure 3A).

To evaluate the performance of the ion-exchange module, we chose eGFP (29 kDa) and BSA (67 kDa) as model proteins, and DEAE Sepharose Fast-Flow (90 µm average diameter), an anion exchanger, as a model medium. After packing the bed with medium and sealing the loading port, we performed a qualitative breakthrough analysis using eGFP. As a solution of eGFP (160 µg/mL) was flowed in, a uniform front of protein, easily visible to the naked eye, advanced steadily across the bed until it was saturated (Figure 3B). Examination of fluorescence intensity in the eluate during breakthrough analysis revealed that capture of eGFP from dilute solution was quantitative, i.e., there was no detectable GFP leaving the column until near the point of saturation. Washing the bed with 2.0 M NaCl resulted in immediate elution of the protein, with a sharp front clearly visible in the device (Figure 3C) and in the fluorescence intensity profile of the eluate (Figure 3D). The tailing in the eGFP peak (Figure 3D) is attributed to fluidic retention at the outlet of the microfluidic module; an oversized outlet chamber surrounding the tubing can act as a mixing chamber between the outlet tubing and the fluidic channel. Tailing should be reduced by size-matching the outlet channel of the microfluidic master and the tubing and minimizing excess dead volume space by using minimal Duco cement during fabrication.

A quantitative breakthrough analysis was repeated with BSA, a common standard, giving a total bed binding capacity of 2.8 mg (measures from two separate modules). For comparison, the manufacturer's literature cites a dynamic binding capacity of 110 mg/mL for human serum albumin (HSA).

Total or dynamic binding capacity is determined by a number of factors. Module volume for IEC beads ~13 µL (11 µL bed volume + ~1-2 µL bead-filled loading port) is defined through design and fabrication. Bead packing density can vary between devices owing to manual manipulation to minimize voids; beads may become more densely packed than what could be achieved through gravity sedimentation alone. Flow rates, contact time, protein sample composition, and buffers (pH and ionic strength) also influence binding capacities and will vary based on experimental conditions. Increased protein concentration on the beads is achieved as the media approaches saturation, but at the expense of recovery. The results of these measures are within expectation for IEC, thus the goal of retaining milligram quantities of protein has been met.

The binding and elution process of non-fluorescent proteins on DEAE Sepharose in microfluidics was visible to the naked eye, as proteins bound to the media, the channels turned opaque. During the elution process, the ion exchange media appearance reverted back to a semi-translucent appearance.

While the demonstration experiments employed an anion exchanger, a variety of separation modules can be produced from the same master by packing the channels with different chromatography media, including metal-affinity media as discussed below. Straightforward modifications to the master would allow, for example, elongation of the bed to increase the binding capacity, thus, there is considerable flexibility to tailor the device for desired elution volumes, target protein quantity, or runtimes.

3.3. Three-dimension (3-D) fluidic bridges.

Implementation of multi-step protein purification strategies in a single device requires a means of connecting and integrating modular purification stages. We developed a novel approach to module integration using customized, cast-in place fluidic bridges. In this approach, acrylonitrile-butadiene-styrene (ABS) copolymer filaments are cemented to the master and then cast into the PDMS. After curing of the polymer and removal of the casting from the master, the ABS filaments are clipped, lubricated with isopropyl alcohol, and withdrawn to leave smooth fluid paths (Figure 4A–E). The process is straightforward, but care must be taken not to cure the PDMS above the glass transition temperature of ABS (~105 °C), nor to cure it for extended periods of time. Excessive cure times and temperatures can cause the filaments to become brittle and fragment upon attempted withdrawal.

Several advantages accrue from the use of sacrificial ABS filaments to create fluidic paths. The filaments are flexible, so it is easy to create curved fluidic bridges around needed features (ports, imaging windows, valves, etc.) to achieve shorter fluidic paths than what would be allowed with a monolithic master. Filaments can be bowed over larger structures (*e.g.*, a wide chromatography module) to prevent fluidic shorts that can result from thin PDMS membranes between the fluidic bridge and the PDMS surface of a channel or the exterior of the device. Furthermore, the use of cast-in-place fluidic interconnects allows multiple device configurations to be created from a single, generic master. The approach does not damage the master, so additional castings can be made using either the same or different fluidic configurations (Figure 4 D–E) with only a minor increase in assembly time. Thus, the fluidic bridges increase the versatility of microfluidic masters and eliminate the need for new masks and for returning to the cleanroom to remanufacture device masters. By extension, the approach could also be used to link multiple masters from different wafers, thus circumventing the scale limit of single-wafer devices for the creation of an integrated platform for biochemical separations.

Our current implementation of the approach introduces some additional dead volume in the fluid path in comparison to what might be achieved using a dedicated master with built-in fluidic interconnects. However use of a dedicated flow path comes at the expense of increased fabrication cost and decreased versatility for each master. By reducing dead volume at the filament termini, our approach can potentially rival the direct-fabrication approach and surpass it where the ability to
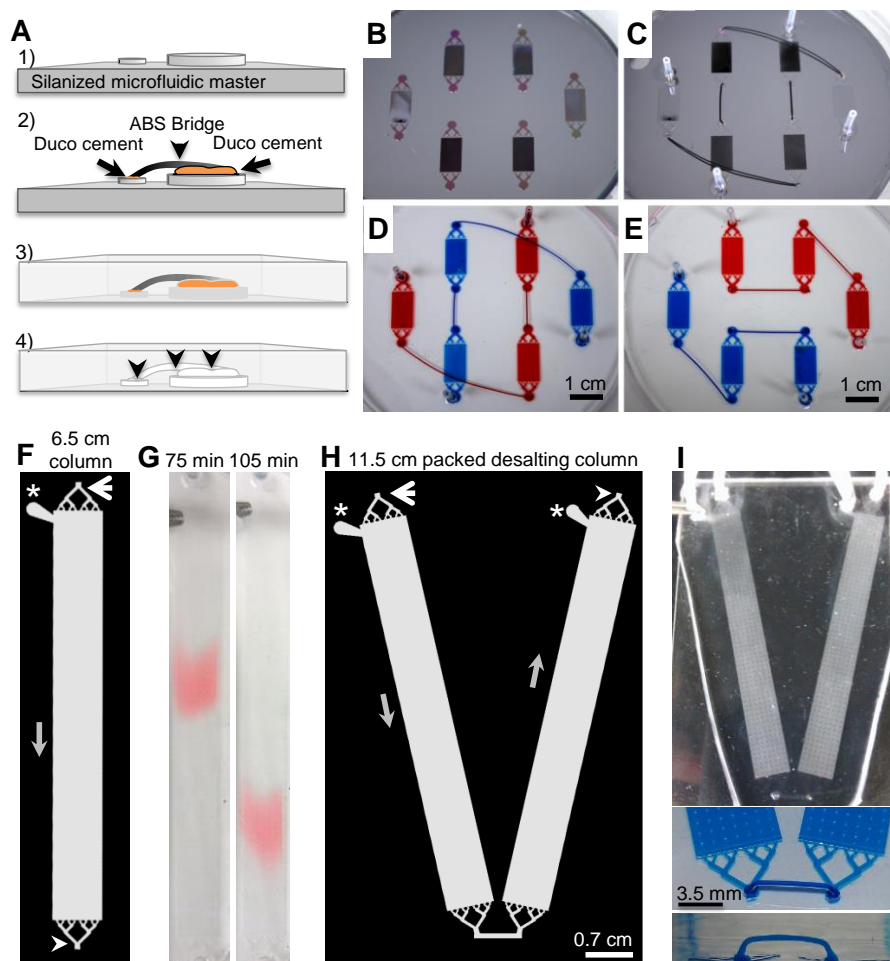
Figure 4. Module customization with fluid paths through 3-D fluidic bridges. A) Process for fabricating integral fluidic bridges. (1) The microfluidic master. (2) ABS filaments reversibly glued between module termini on the master with Duco Cement. Silastic tubing (not shown) is glued to ports. (3) PDMS pre-polymer is poured onto the master and cured. (4) After the microfluidic master is separated, Duco cement and ABS filaments are removed from the cured PDMS to leave fluidic channels (arrows). B) Image of a master containing microfluidic modules, step A1. C) Image of the master under cured PDMS with embedded ABS filament and Silastic tubing, step A3. D-E) Two different microfluid paths after removal of ABS filaments and Duco cement. Red or blue dyes were injected into the two independent paths. F-I) Coupling SEC modules with 3-D fluidic bridges. F) Schematic of single bed SEC module [7.0 cm (*l*), 0.7 cm (*w*) and 0.013 cm (*d*), 64 μL channel volume]. G) Red 40 band (5 μL) migration in microfluidic SEC module (7.0 cm long channel, 6.5 cm long final packed bed (sieved Sephadex G-25 resin)) illustrating the uniformity of migration under flow (50 μL/h) at two time points (75 and 105 min). H) Schematic of coupled tandem beds (11.5 cm total bed length, 128 μL total bed volume, 1.37 μL bridge). Column inlets (white arrows) distribute fluid evenly across the width of the device through series of bifurcating channels. The media loading port (*), column outlet port (chevron), and flow direction (grey arrow) are indicated. I) Module of tandem SEC beds. Top: photograph of device. Middle: close-up image of dye-filled fluidic bridge, channel support posts are observed in the device. Bottom: Side view of fluidic bridge (7 mm) between inlet and outlet.

work in three dimensions leads to shorter flow paths between points on a master, or connect separate masters (Figure 4F-I).

3.4. Size-exclusion chromatography (SEC) modules.

SEC is a common technique that can be used for macromolecular separations but is also useful for rapid desalting and buffer exchange of protein solutions. The latter application was of interest in the present context because it provides a useful means for bridging chromatographic modalities that require different buffer conditions. Furthermore, it provides an effective polishing step for proteins purified by ion-exchange or affinity chromatography that are substantially pure except for salts and ligands used to elute them. In comparison to IEX, SEC has a lower capacity per unit volume

and is more sensitive to chromatographic conditions, particularly bed dimensions and flow rate. Typical SEC beds are long and narrow, with aspect ratios (length/width) often being 10 or more. Figure 4F-I summarizes the two SEC module architectures that allowed for aspect ratios of 10 and 17. Initially, we fabricated microfluidics for SEC beds that were 7 cm long and 0.7 cm wide (Figure 4F-G); column length was restricted (≤ 7 cm) due 10-cm wafer requirements. To create longer beds for greater capacity or improved separation, we coupled two beds on a wafer while keeping the connections between the separation channels as short as possible (Figures 4H-I). To make room for short interconnects between the modules, each channel size needed to be reduced from 7 cm to 6 cm in length. Rather than connecting the two size-exclusion
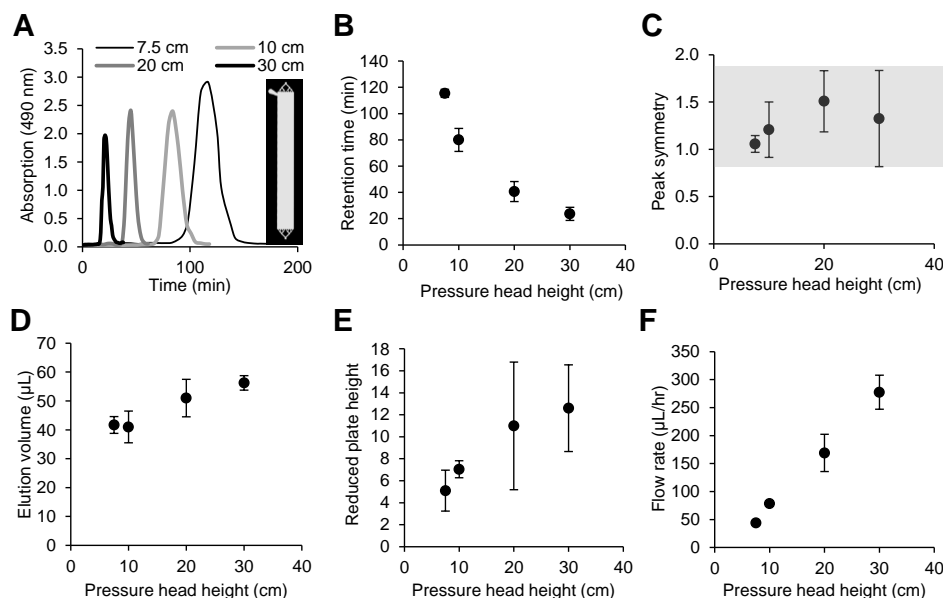
Figure 5. Flow performance of the packed 6.5-cm single-bed, SEC module (5 µL sample vol., 60 µL packed bed vol.) using Red 40 (MW = 496). A) Peak profiles for gravity-induced flow over a range of pressure head heights from 7.5–30 cm. Inset: single bed schematic. B) Retention time for Red 40 as a function of head height. C) Peak symmetry as a function of head height. Mean values (± SD) fell within a typical range (grey zone) for conventional SEC systems. D) Elution volume as a function of head height E) Reduced plate height as a function of head height. F) Flow rate as a function of head height. Calculated flow rates (µL/min) for pressure head heights were used for adopting syringe pumps for matching flow rates in modules with longer channels of packed media.

columns within the architecture defined by lithography, we implemented fluidic cast-in-place fluidic bridges (discussed above) to minimize the fluid path between modules and enable customization of module sequence within or between wafers.

Ideally, a single, contiguous column bed eliminates difficulties associated with column-to-column sample transfer; however, due to the fabrication space restrictions of a 4-inch wafer for constructing a single linear column (> 11 cm), coupling two microfluidic columns allowed for an increased separation bed (Figure 4H-I).

We next characterized flow performance of single channel size-exclusion devices, and then assessed both 6.5 cm and 11.5 cm beds for peak separation of salt and proteins. To observe flow characteristics, assess performance qualitatively, and measure peak profiles quantitatively, we used the dye Red 40 (M_R 496) as a model analyte in microfluidic beds packed with Sephadex G-25. For each run, a 5-µL plug of dye solution was loaded, and flow was induced through the column using static pressure head at a series of head heights from 7.5 to 30 cm. Figure 4G shows the migration of a uniform, red band through the bed. We anticipated that serially connecting two separation beds through fluidic bridges (Figure 4I, bottom two images) could impact separation performance, however, the tradeoff would be increased protein and salt separation given that the total length of the separation column is nearly doubled.

Figure 5 shows the effects of flow rate on several chromatographic properties for Red 40 processed in the single 6.5 cm module. Retention time and peak symmetry values are shown in Figure 5A-C. The elution volume (Figure 5D) is the

volume of the Red 40 peak. Reduced plate height values are used to measure column efficiency (Figure 5E). The values for flow rate (Figure 5F) for the respective pressure head height were determined for extending the range of flow controls through the use of syringe pumps. Flow rate exhibited a linear dependence on pressure head, and the peak consistently eluted in a volume of 40–60 µL (Figure 5D), the single channel flow characterization (Figure 4G and 5A-C) is modified from prior presentation.[37] Asymmetry factor determinations fell within the range of 0.8–1.8 and were on average near 1.3; for reference, the asymmetry factor in a conventional column should fall in the range of 0.7-1.3. Large asymmetry factors (> 1) indicate peak tailing, which in the present case probably resulted from dead volume in the fluidic path inlet and outlet, as discussed above. Faster mobile flow rates did not on average worsen asymmetry but did increase the range of asymmetry values in replicate analyses (Figure 5C). In contrast, increasing flow rate adversely affected separation quality, as reflected in the reduced plate height. At the slowest flow rate (7.5 cm head), the average reduced plate height of ~5 approached a level that would be considered very good for SEC media (< 3). Overall, the bed displayed performance approaching that of a well-packed conventional SEC column. Having established that the benchmark performance of the single bed device was satisfactory, we assessed the tandem-bed, 11.5-cm module for performance in protein desalting. Hydrostatic pressure from fluidic pressure head columns was insufficient to induce the higher flow rates of Figure 5F in the two-bed module. To overcome this limitation and deliver precise flow rates that
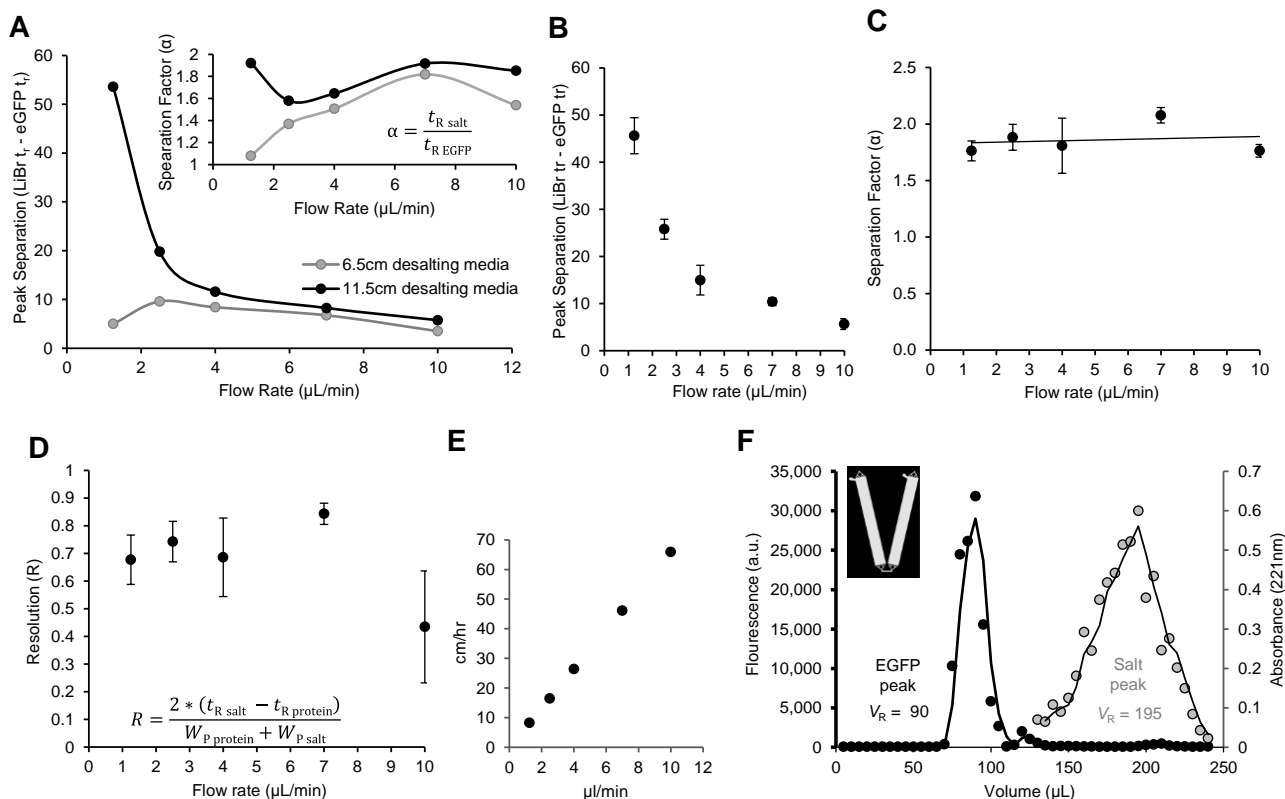
Figure 6. Performance of size-exclusion modules for desalting proteins. (A) Peak separation is the difference (LiBr t_R - EGFP t_R) between salt only (1.6 M LiBr) and protein only (21 µg EGFP) peaks from control solutions using 6.5 cm and 11.5 cm microfluidic size-exclusion modules. Inset, same control data represented by separation factor alpha. (B) Peak separation from LiBr+EGFP mixtures separated using 11.5 cm module. Results are similar to simple solutions shown in (A). Inset graph: flow rate conversion between cm/hr and µL/min. C-D) Chromatographic performance as a function of flow rate assessed for a protein–salt mixture. Samples (10 µL) of eGFP (21µg) in 1.6 M LiBr loaded onto the 11.5-cm tandem-bed module and eluted at the indicated flow rates. In C) the separation factor α is shown, whereas in D), the resolution R takes peak-width into consideration. (E) Flow rate conversions. (F) Representative chromatograms for protein (21 µg eGFP) and salt (1.6 M LiBr) separated and eluted (1.25 µL/min) using the tandem (11.5 cm) SEC module (sieved Sephadex G-25), 3 h run time. Sample volume (30 µL) was 27% of the bed volume of 110 µL, reflecting the practical capacity limit for SEC. eGFP elutes in the void (V_R = 90 µL), whereas LiBr is sieved and elutes later (V_R = 195 µL).

were independent of device configuration, we implemented active flow control with syringe pumps.

As model analytes, we chose eGFP and LiBr. Both are easily detected and quantified on small scale, the former by several methods and the latter by absorbance of the bromide ion at 221 nm. The performance of the 6.5 and 11.5 cm size-exclusion modules for desalting proteins was assessed first by separately measuring the retention times of control solutions consisting of either EGFP protein or LiBr salt. Figure 6A shows the difference in retention times (LiBr t_R - EGFP t_R) between salt only (1.6 M LiBr) and protein only (21 µg EGFP) peaks (10 µL loading volumes each). The separation factor (α) is a ratio of retention times (LiBr t_R / EGFP t_R) indicating quality of separation, a larger (α) value indicates better separation. At low flow rates (1.25 µL/min) the 11.5 cm module appears to outperform the 6.5 cm module.

We applied the separation conditions, determined from simple solutions (Figure 6A), to desalting protein-salt mixtures. Mixed samples (10 µL) of eGFP+LiBr were separated for the same flow rates in the 11.5 cm module (Figure 6B). Peak separations (Figure 6B) are in agreement with control measures

(Figure 6A), indicating our assay methodology for small volumes allow peak observation and that LiBr does not interact or confound the separation of this fluorescent protein mixture.

Performance was assessed quantitatively in terms of separation factor (α) and resolution (R) over a range of flow rates from 1–10 µL/min (~6–60 cm/hr linear velocity) using separate, 10-µL injections of eGFP solution or 1.6 M LiBr. As shown in Figure 6C, the separation factor was consistently ~1.8, which is comparable to expectations for a conventional column. Resolution was consistently about 0.75 at flow rates up to 7.5 µL/min but dropped at 10 µL/min (Figure 6D) The resolution of 0.75 is comparable to, but somewhat less than, what would be expected for a well-packed conventional column ($R ≈ 1–2$) but is sufficient to separate protein from salt with <10% peak overlap. This result suggests that the 1.37 µL fluidic bridge permits the ability to desalt a protein product. The comparison of two conventional flow parameters is shown (Figure 6E). Figure 6F shows that this expectation is born out in practice with a representative separation of eGFP and LiBr using the 11.5-cm, tandem-bed device. While the fluidic bridge may increase band broadening, figure 6F shows good product

Integrated affinity capture and SEC modules
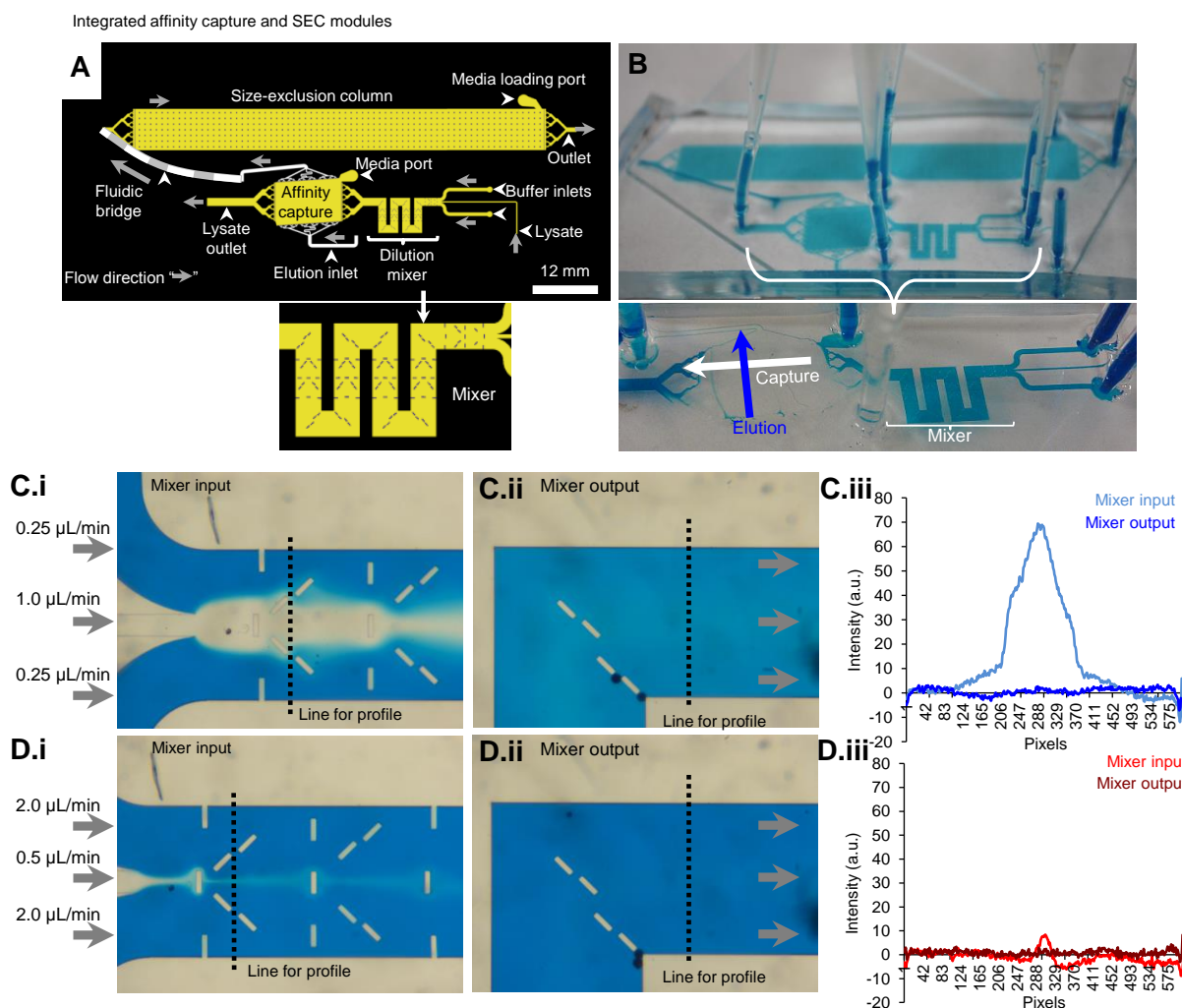
Figure 7. Characterization of integrated IMAC capture and SEC modules for enrichment of eGFP from crude *E. coli* cell lysate. A) Overview of the microfluidic architecture for protein capture, affinity purification and desalting. Cell lysate is diluted in the mixer channel (32 mm long) for selective protein capture on IMAC media. After washing, elution transfers captured protein through a 5.1 μL fluidic bridge into the SEC buffer exchange module, from which it is collected. Outset image: detail of the mixer channel. B) Image of the unpacked, integrated device filled with blue dye; outset image shows removal of dye through cross-flow elution. C-D) Mixer input channels where buffer channels combine with cell lysate channels for mixing. C.i.-D.i.) Left images show input streams and flow rates. C.ii.-D.ii.) Middle images show the mixer output from corresponding inputs (left) acquired under steady state flow. C.iii-D.iii) Graphs of input/output flow profile (dashed lines) are shown, blue line profiles are from (C), red lines from (D).

separation; it is noteworthy to identify that the fluidic bridge is ~1% (1.37 μL) of the 128 μL total bed volume. Ideal sample loading volumes for size-exclusion separation are typically 30% of the column volume; smaller volumes (< 25% of column volume) typically perform better than larger loading volumes (> 30% column volume) that can approach media saturation. Qualitatively complete separation of protein from salt was obtained from a 30-μL sample (~25% of bed volume) containing 21 μg of eGFP and 1.6 M LiBr.

3.5. Protein purification with integrated IMAC/SEC modules.

Having validated IEX and SEC modules separately and developed a simple method to interconnect them, we sought to apply these modules to the purification of a recombinant protein. As a model protein, we chose His-tagged eGFP

expressed in *E. coli*, which can be purified by immobilized-metal affinity chromatography (IMAC) followed by desalting through SEC. IMAC is operationally similar to IEC, and thus either mode can be employed in the same device. The process flow for the integrated platform for performing the purification, illustrated in Figure 7, involves (1) injection of *E. coli* lysate containing recombinant, His-tagged eGFP, (2) dilution through a fluidic mixer, (3) capture of the protein on Co^{2+}-NTA resin (4) washing to remove non-specifically bound proteins (5) elution with imidazole using perpendicular-flow directly into the SEC module, and (6) recovery of the purified protein from a single-bed SEC module (Figure 7A). Integration for optimized separation and maximum yield, and purity, will require scaling modules to match fluidic handoff between modules.

New features introduced to accomplish serial purification

Lab on a Chip Accepted Manuscript

were a cross-flow IEC/IMAC bed to provide orthogonal streams for sample and waste and an inlet dilution mixer (Figure 7). The cross-flow bed has microporous barriers with branched distribution/collection channels on all four sides. Flow control for capture and cross-flow elution with this valve-less architecture is achieved by differential positive pressures, an approach which also minimizes bubble formation in chromatography beds and prevents cross-module contamination. The inlet mixer was introduced to facilitate sample loading, washing and elution. IEC often requires dilution of the sample to reduce ionic strength and promote binding, followed by elution at higher ionic strength. In IMAC, washing is required to elute non-specifically-bound protein species prior to elution of the specifically bound protein with buffer containing a competing ligand, e.g., imidazole.

We designed a microfluidic mixer for IEC that functions as a stream-switching inlet port for changing buffers during separation by IEC or IMAC, eliminating the need for plumbing changes on the inlet side. The design combines serpentine mixing and passive planar micromixers[38] to merge three streams efficiently. In the example shown, the sample stream accounts for 20% of the cross sectional channel volume and two independent buffer streams account for the remaining 80%. By modulating flow rates of the inlet streams, one can select for any single stream or generate binary or ternary mixtures, including gradients. Through profile analysis of mixer inlet and outlet images acquired from a series of tested flow rates, we verified that complete mixing of sample and buffer streams was achieved at the IEC/IMAC module outlet (Figure 7). Optimal dilution and mixture are achieved within the mixing module when the flow rate of the central (lysate) channel (0.5 µL/min) was kept low relative to the flow rate of the side (buffer) channels (2.0 µL/min).

With the device in hand and the beds packed, the separation process was performed as follows. Lysate (~120 µL) was loaded onto the IMAC bed at a flow rate of 4 µL/min. During this time, the two inlet buffer streams were filled with IMAC buffer (without imidazole, MCAC0). At the same time, the SEC module was flushed in reverse at a lower flow rate (1 µL/min) to prevent lysate or IMAC flow-through from entering the fluidic bridge to the SEC column (Figure 8A); the affinity elution inlet was also perfused with a flow rate matched with the SEC module using a dual syringe pump (1 µL/min). After all of the sample had been loaded, the IMAC module was rinsed with buffer through both buffer ports (4 µL/min, combined flow) containing a low concentration of imidazole (0.02 M) to remove non-specifically bound proteins. Subsequently, the IMAC media was rinsed, eluted, and cleared of protein, under buffer stream flow or elution cross-flow (4 µL/min), with step concentrations of imidazole (0.02-1.0 M) buffer. Rinsing buffer streams of MCAC0 and 0.02 M imidazole were eluted into the lysate outlet as waste streams.

During elution, 0.06 M imidazole buffer containing eGFP was eluted directly into the SEC bed for desalting (Figure 8B) with the lysate outlet and buffer inlets providing slight positive
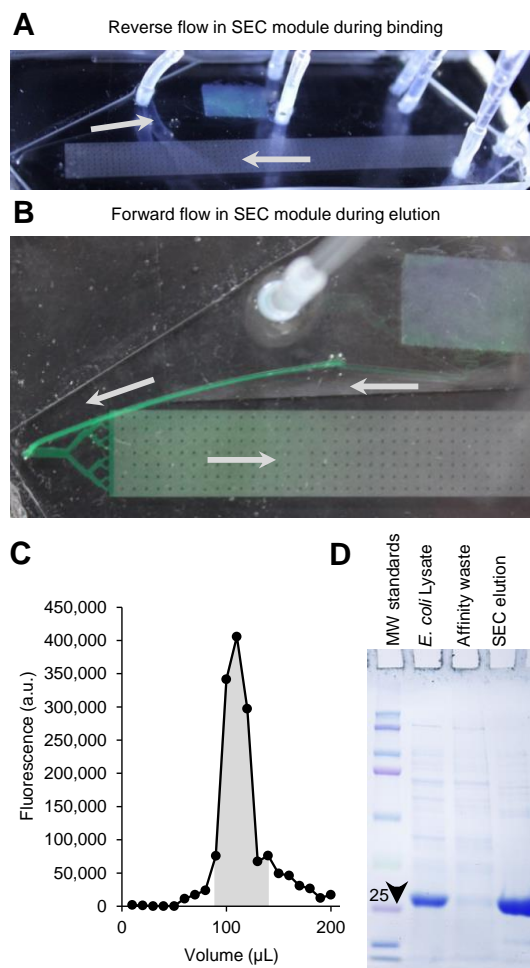
Figure 8. Enrichment of eGFP with integrated IMAC and SEC modules. A) Photograph of packed, IMAC and SEC modules for affinity capture of eGFP on Co^{2+}-NTA resin. B) Elution of His-tagged eGFP from the affinity module directly onto size-exclusion module (containing Sephadex G-25) through the embedded 3-D fluidic bridge. Arrows indicate flow direction. C) Chromatogram showing the elution of eGFP from the integrated IMAC/SEC module. Measured yield of pooled six fractions (grey shading) was 275 µg. D) Analysis of protein purity by SDS-PAGE showing the effective capture, purification and concentration of eGFP from *E. coli* cell lysate. Comparison of the lysate, IMAC flow-through and purified protein shows substantial purification and concentration. His-tagged eGFP M_r = 29 kDa, 25 kDa standard band (arrow at 25).

flow (1 µL/min) to prevent backflow. Eluate from the SEC module was collected in 10 fractions of 10 µL, each. The majority of the protein eluted in 6 fractions (Figure 8C), which were pooled to yield 4.6 mg/mL eGFP protein concentrated out of 112 µL *E. coli* lysate.

Of the many analytical measures (e.g. mass spec, western blot, gel electrophoresis) for protein recovery and purification, SDS-PAGE was used to confirm increased purity and concentration of eGFP from the integrated chromatography platform (Figure 8D). For perspective, during our IEC device characterization studies, 650 µg eGFP was captured and eluted into 35 µL (Figure 3D); in the integrated IMAC module, eGFP was captured and eluted into and SEC column for desalting to yield 275 µg in 60 µL out of the integrated module. The total process time for this module is between 1.5 to 2.25 hours.

4. Conclusions

In this work, we have introduced a new microfluidic platform for small-scale protein purification using coupled chromatographic separations. Distinctive features of the platform include microporous barriers to retain chromatography media and cast-in-place fluidic interconnects formed around sacrificial ABS filaments. After demonstrating that both IEC and SEC could be performed in microfluidic beds, with separation quality approaching that of conventional column chromatography, we created a device integrating IMAC and SEC modules to purify 275 μg of His-tagged eGFP from 773 μg crude *E. coli* cell lysate. The integrated device incorporated a dilution mixer at the sample inlet and a cross-flow bed in the IMAC module to facilitate protein capture, washing and elution.

To improve separation capacity and quality, future modifications to the fluidic architecture could reduce dead volume, integrate valves to improve stream switching, and improve sample handling through the mixer and affinity modules. These improvements would increase the speed and capacity of the device while improving the yield and purity of the protein product. Due to the modular nature of the architecture and the ease with which modules can be interconnected, further refinements can be made to incorporate additional chromatographic steps scale-matched to the sample mass and volume at each step in the separation. In this way, fully automated delivery of microgram to milligram quantities of pure protein isolated from crude sources can be realized.

Acknowledgements

References

1   A. De Luminy and M. Cedex, *Nat Methods*, 2008, **5**, 135–146.
2   F. Bernhard and Y. Tozawa, *Curr. Opin. Struct. Biol.*, 2013, **23**, 374–380.
3   L. J. Millet, A. Bora, J. V Sweedler and M. U. Gillette, *ACS Chem Neurosci*, 2010, **1**, 36–48.
4   M. J. Jebrail and A. R. Wheeler, *Anal. Chem.*, 2009, **81**, 330–335.
5   G. Rosenblum and B. S. Cooperman, *FEBS Lett.*, 2014, **588**, 261–268.
6   S. Rupp, *Eng. Life Sci.*, 2013, **13**, 19–25.
7   C. J. Murray and R. Baliga, *Curr. Opin. Chem. Biol.*, 2013, **17**, 420–426.
8   J. F. Zawada, G. Yin, A. R. Steiner, J. Yang, A. Naresh, S. M. Roy, D. S. Gold, H. G. Heinsohn and C. J. Murray, *Biotechnol. Bioeng.*, 2011, **108**, 1570–1578.
9   M. G. Casteleijn, A. Urtti and S. Sarkhel, *Int. J. Pharm.*, 2013, **440**, 39–47.
10   V. Gubala, L. F. Harris, A. J. Ricco, M. X. Tan and D. E. Williams, *Anal. Chem.*, 2012, 84, 487–515.
11   G. J. Kost, N. K. Tran, M. Tuntideelert, S. Kulrattanamaneeporn and N. Peungposop, *Am. J. Clin. Pathol.*, 2006, **126**, 513–520.
12   T. Lai, Y. Yang and S. K. Ng, *Pharmaceuticals (Basel).*, 2013, **6**, 579–603.
13   P. Siuti, S. T. Retterer, C.-K. Choi and M. J. Doktycz, *Anal. Chem.*, 2012, **84**, 1092–7.
14   S. T. Retterer, P. Siuti, C.-K. Choi, D. K. Thomas and M. J. Doktycz, *Lab Chip*, 2010, **10**, 1174–1181.
15   M. S. Shapiro, S. J. Haswell, G. J. Lye and D. G. Bracewell, *Biotechnol. Prog.*, 2009, **25**, 277–285.
16   M. S. Shapiro, S. J. Haswell, G. J. Lye and D. G. Bracewell, *Sep. Sci. Technol.*, 2011, **46**, 185–194.
17   S. Gerontas, M. S. Shapiro and D. G. Bracewell, *J. Chromatogr. A*, 2013, **1284**, 44–52.
18   I. M. Lazar, P. Trisiripisal and H. A. Sarvaiya, *Anal. Chem.*, 2006, **78**, 5513–5524.
19   L. C. Taylor, N. V Lavrik and M. J. Sepaniak, *Anal. Chem.*, 2010, **82**, 9549–9556.
20   N. V Lavrik, L. T. Taylor and M. J. Sepaniak, *Anal. Chim. Acta*, 2011, **694**, 6–20.
21   K. S. Deshpande, S. Kuddannaya, J. Staginus, P. C. Thüne, L. C. P. M. de Smet, J. H. ter Horst, L. a. M. van der Wielen and M. Ottens, *Biochem. Eng. J.*, 2012, **67**, 111–119.
22   R. Hu, X. Feng, P. Chen, M. Fu, H. Chen, L. Guo and B. F. Liu, *J. Chromatogr. A*, 2011, **1218**, 171–177.
23   D. A. Annis, E. Nickbarg, X. Yang, M. R. Ziebell and C. E. Whitehurst, *Curr. Opin. Chem. Biol.*, 2007, 11, 518–526.
24   M. D. Duong-Thi, E. Meiby, M. Bergström, T. Fex, R. Isaksson and S. Ohlson, *Anal. Biochem.*, 2011, **414**, 138–146.
25   L. Kang, B. G. Chung, R. Langer and A. Khademhosseini, *Drug Discov. Today*, 2008, 13, 1–13.
26   *Strategies for Protein Purification – Handbook. GE Healthcare, 28-9833-31 AA, 09/2010*, .
27   A. Nordborg and E. F. Hilder, *Anal. Bioanal. Chem.*, 2009, 394, 71–84.
28   G. Chirica, J. Lachmann and J. Chan, *Anal. Chem.*, 2006, **78**, 5362–5368.
29   V. VanDelinder and A. Groisman, *Anal. Chem.*, 2006, **78**, 3765–3771.
30   Y. Sai, M. Yamada, M. Yasuda and M. Seki, *J. Chromatogr. A*, 2006, **1127**, 214–220.
31   Q. Zhao, M. Wu, X. Chris Le and X. F. Li, *TrAC - Trends Anal. Chem.*, 2012, 41, 46–57.
32   F. A. Gomez, *Methods Mol. Biol.*, 2011, **681**, 137–150.
33   X. Cheng, D. Irimia, M. Dixon, K. Sekine, U. Demirci, L. Zamir, R. G. Tompkins, W. Rodriguez and M. Toner, *Lab Chip*, 2007, **7**, 170–178.
34   C. A. Croushore, S. Supharoek, C. Y. Lee, J. Jakmunee and J. V Sweedler, *Anal Chem*, 2012, **84**, 9446–9452.
35   M. Nič, *IUPAC Compend. Chem. Terminol. Gold B.*, 1997, **2**, 1997–1997.
36   K. J. Petty, *Metal-chelate affinity chromatography.*, .
37   L. J. Millet, S. T. Retterer and M. J. Doktycz, *Proc. Micro Total Anal. Syst. 2014, San Antonio, Texas, USA.*, 2014.
38   A. A. S. Bhagat and I. Papautsky, *J. Micromechanics Microengineering*, 2008, **18**, 085005.

Lab on a Chip Accepted Manuscript